PCCP

Dynamics of molecular associates in methanol/water mixtures

Journal:	*Physical Chemistry Chemical Physics*
Manuscript ID	CP-ART-10-2021-004726.R1
Article Type:	Paper
Date Submitted by the Author:	14-Dec-2021

Complete List of Authors:	Zhai, Yanqin; University of Illinois at Urbana-Champaign, Luo, Peng; UIUC, Beckman Institute for Advanced Science and Technology Waller, Jackson; North Carolina State University Self, Jeffrey; University of California Santa Barbara Harriger, Leland; National Institute of Standards and Technology Y, Z; University of Illinois at Urbana-Champaign, Nuclear, Plasma, and Radiological Engineering, Department of Materials Science and Engineering, Department of Electrical and Computer Engineering Faraone, Antonio; NIST,

Journal Name

ARTICLE TYPE

Cite this: DOI: 00.0000/xxxxxxxxxx

Dynamics of Molecular Associates in Methanol/Water Mixtures†

Yanqin Zhai,[ab] Peng Luo,[b] Jackson Waller,[c] Jeffrey L. Self,[de] Leland W. Harriger,[f] Y Z*[abg] and Antonio Faraone*[f]

Received Date
Accepted Date

DOI: 00.0000/xxxxxxxxxx

The dynamics of molecular associates in methanol/water mixtures was investigated using quasielastic neutron scattering. By measuring the signal from four methanol/water samples differing only by their isotopic composition, the relative motion of the water to methanol molecules, i.e. their mutual dynamics, was determined at the nanoscale. The thus obtained nanoscopic mutual diffusion coefficient signals a significantly slower process than the single particle diffusion of either methanol or water in the system as well as their macroscopic mutual diffusion. The data do not provide any indication of microsegregation in this preeminent alcohol/water mixture; however, they do indicate the existence of long lived but dynamic molecular associates of water and methanol molecules. Analysis of the structural relaxation shows that the lifetime of molecular association through hydrogen bonding determines the fact that viscosity of the mixtures at intermediate concentrations is higher than that of both pure components.

1 Introduction

Non-ideal mixing in alcohol/water solutions, with their thermodynamic anomalies such as the volume reduction and the heat release during mixing as well as abnormalities of their transport properties such as viscosity-composition maxima, has attracted scientific attention for decades.[1] This behavior has been associated to nanoscopic structural phenomena, in otherwise macroscopically homogeneous liquids, such as hydrophobic effects (structuring of water molecules around a hydrophobic moiety),[2–4] microsegregation,[5] and even micellization.[6] In fact, mesoscopic structuring in mixtures of associating liquids is still a topic of active research.[7] In particular, methanol/water solutions have attracted much attention for many years and continue to attract interest,[8] sometimes for reasons beyond the thermodynamic and transport anomalies of the mixture, such as to study the low temperature properties of water avoiding freezing.[9,10] In fact, methanol with a hydroxyl head and a methyl tail can be considered the simplest amphiphile; as such, methanol/water mixtures can be considered prototypical of alcohol aqueous solutions. In these mixtures, the behavior of the excess entropy of the mixture as a function of methanol concentration has long been considered a strong indication of molecular structuring. However, whereas for longer alcohols[6] or alcohols with bulkier hydrophobic groups[11] scattering methods provide clear evidence of aggregated complexes, for methanol/water distinguishing between the concentration fluctuations and microsegregation or micellization phenomena is challenging. Nevertheless, the idea that clusters of methanol molecules could be present in the mixture and be the origin of the anomalous thermodynamic behavior has been put forward,[5] on the basis of a combined effort with computer simulation and neutron diffraction. Similar segregation phenomena have been hypothesized, for example, in tert-butyl alcohol/water mixture which show evidence of mesoscale inhomogeneities.[11,12] On the other hand, recent x-ray scattering results indicate extensive hydrogen bonding association between water and methanol molecules.[13]

Beyond alcohol/water mixtures, the topics of microsegregation and association are of great interest for other liquids which present intermediate range structuring such as, for example, ionic liquids (IL),[14,15] deep eutectic solvents (DES),[16,17] and superconcentrated electrolytes, commonly called water-in-salt (WIS),

[a] Department of Nuclear, Plasma, and Radiological Engineering, University of Illinois at Urbana-Champaign, Urbana, Illinois 61801, USA
[b] Beckman Institute for Advanced Science and Technology, University of Illinois at Urbana-Champaign, Urbana, Illinois 61801, USA
[c] Department of Physics and Mathematics, North Carolina State University, Raleigh, North Carolina 27695, USA
[d] McKetta Department of Chemical Engineering, University of Texas at Austin, Austin, Texas 78712, USA
[e] Current address: Department of Chemistry and Biochemistry, University of California Santa Barbara, Santa Barbara, CA 93106-9510, USA
[f] NIST Center for Neutron Research, National Institute of Standards and Technology, Gaithersburg, Maryland 20899, USA
[g] Department of Electrical and Computer Engineering, University of Illinois at Urbana-Champaign, Urbana, Illinois 61801, USA
* E-mail: zhyang@illinois.edu; afaraone@nist.gov

† Electronic Supplementary Information (ESI) available: [details of any supplementary information available should be included here]. See DOI: 00.0000/00000000.

which hold great promises for the development of the next safe and sustainable electrochemical devices.[18,19]

Experimentally, methanol/water solution have been investigated using a number of different techniques. Naturally, much attention has been paid to the structure of the system at the molecular level.[13,20,21] However, much work has been devoted also to the investigation of its dynamical properties. As far as the relaxational dynamics in the system is concerned, a series of papers have been published on the single particle dynamics of methanol and water using both Pulse Gradient Spin Echo Nuclear Magnetic Resonance (PGSE-NMR)[22–24] and QuasiElastic Neutron Scattering (QENS)[25] measurements of the incoherent component of the spectra.[26] These studies have put in evidence the temperature dependence of the interplay between hydrophilic and hydrophobic interactions in the mixtures.[10,24] The results suggest an increased tendency to segregation as temperature is lowered. Anomalous behavior, such as the cross-over from a super Arrhenius to Arrhenius behavior at a temperature of ≈225 K as well as the breakdown of the Stokes-Einstein relation,[24] was reported.[23] These findings where interpreted in terms of the hypothesized second critical point of water;[23] although the presence of small crystallites has been also suggested.[26]

In these mixtures, the mutual dynamics of methanol and water at the molecular level is much less known. However, an understanding of the nature of the nanoscopic structures as well as of the abnormal behavior of the transport properties in methanol/water, necessitates information on the relative motion of the methanol-water, water-water, and methanol-methanol pairs. A possible experimental techniques to gain such information is QENS measurements focusing on the coherent component of the spectra. This scattering technique gives information on the relaxation time of the correlation of couples of atoms in the system at the nanometer length scale on a time scale ranging from few picoseconds up to several nanoseconds. However, the effectiveness of this kind of experiments for the investigation of association and microsegregation is often limited by several technical factors. In particular, the neutron coherent scattering signal is concentrated at specific exchanged wavevector Q values which probe very specific characteristic length scales in the system, most commonly the interparticle distance at the First Sharp Diffraction Peak (FSDP). This can be very valuable but it might not be what is needed for the understanding of specific structuring in the system. Moreover, several couples of atoms contribute to the coherent signal which might complicate the interpretation of the data, especially when the support of computer simulation is not available.

In an effort to overcome the above mentioned issues, the combination of the data from systems differing only by their isotopic composition can be employed.[17,27–31] The use of isotopic substitution is very common in neutron scattering, because the scattering cross section differs for different isotopes of the same atom, most notably for hydrogen and deuterium. In particular, for structural studies with neutron diffraction, extensively performed for methanol/water mixtures, the combination of data from samples with different isotopic composition allows the optimization of the parameters used for the computer simulation of the system, eventually providing a very detailed structural picture of the system which is in satisfactorily agreement with a wealth of experimental neutron diffraction data. However, for dynamics studies this kind of recursive optimization of, for example Molecular Dynamics (MD) simulations, parameters on the basis of QENS experimental results has not been implemented yet. Usually, isotopic substitution methods in QENS[25] are used to obtain data originating from the incoherent scattering of a specific subset of hydrogen atoms in the system. However, it can be shown[27–31] that by combining the signal from samples differing by their isotopic composition, the incoherent scattering of the samples can be eliminated completely, with the result of obtaining spectra originating from the coherent scattering of a specific subset of atom couples in the system. Such signal would not be usually accessible because of the dominating presence of the incoherent scattering. This method is valid for static scattering but is most relevant for dynamic scattering works aimed at the study of collective dynamics.

In the present work using this method, the mutual dynamics of the water/methanol molecular associates was investigated to determine their lifetime and relation to the macroscopic transport properties. MD simulation provides further support to the interpretation of the obtained results.

The following sections 2 and 3 of the paper describe in details the employed materials and method as well as the underlying theory of neutron scattering . Section 4 reports the experimental results obtained from the structural and dynamic techniques employed; subsection 4.1 focuses on molecular structuring, whereas subsection 4.2.1 and 4.2.2 deal with the mutual diffusion of the molecular species and the structural relaxation, respectively. The final section of the paper is devoted to the conclusion.

2 Materials and Methods

2.1 Samples

Fully deuterated (CD_3OD, D 99.8 % purity) and hydroxyl partially deuterated (CH_3OD, D 99.5 % purity) methanol were purchased from Sigma-Aldrich. Methyl partially deuterated methanol (CD_3OH, D 99.8 % purity) was purchased from CDN isotopes. Deuterium oxide (D_2O, D 99.9 % purity) was purchased by Cambridge Isotopes. Hydrogenated methanol was purchased from Sigma-Aldrich. Liquids were used without further purification. Four methanol water mixture were prepared: CD_3OD/D_2O (S1), CH_3OD/D_2O (S2), CD_3OH/H_2O (S3), and CH_3OH/H_2O (S4). All mixtures had a methanol molar fraction $x_M = 0.54$ and were prepared gravimetricaly. Care was taken that the uncertainty of the methanol molar fraction was of the order of 0.1 %. The molar fraction $x_M = 0.54$ was chosen to allow significant cooling of the sample (below 200 K) without crystallization, in order to investigate the temperature dependence of the dynamics. At this concentration a number of experimental studies have also been published,[10,32] which allows for a critical comparison of the present results. Additional purely structural measurements were performed on samples with $x_M = 0.25$ and $x_M = 0.75$.

2.2 Instrumentation

For the Small Angle Neutron Scattering (SANS) measurements the samples, with a thickness of 0.12 mm determined by a teflon spacer, were sandwiched between quartz windows in titanium demountable cells. For all other experiments the samples were contained in aluminum cans which were sealed with indium. In the aluminum can the sample had a cylindrical geometry and the sample thickness was 0.08 mm.

SANS measurements were performed at room temperature. In all other experiments the temperature was controlled using a cold cycle refrigerator in the range from 300 K to 200 K, with an accuracy of ≈ 1 K.

All neutron scattering measurements were performed at the Center for Neutron Research (NCNR) of the National Institute of Standards and Technology (NIST), Gaithersburg, MD, USA. SANS measurements were performed on the 30 m instrument on Neutron Guide (NG)-7.[33] Diffraction measurements were carried out using the cold triple axis spectrometer SPINS on NG-5. Time-of-Flight (ToF) QENS measurements were performed using the Disk Chopper Spectrometer (DCS) on NG-4.[34] Finally, Neutron Spin Echo (NSE) experiments were performed using the instrument which was installed at the end position of NG-5.[35]

The SANS experiment was performed using an incoming wavelength $\lambda = 5$ Å with a $\Delta\lambda/\lambda \approx 15$ %. The sample detector distance was 1 m. The beam size was reduce to 1.27 cm (0.5 inches) to maximize the accessible scattering angle, without interference from the sample container. Detector efficiency was calculated using a measurement on a standard polymeric sample. Scattering from the direct beam was used to reduce the data to absolute intensity, using routines available from NCNR[36].

The SPINS spectrometer was operated in the two axis mode with an incoming wavelength of 4.04 Å. A measurement from a standard vanadium sample was used to correct for geometrical instrumental effects in the measurement of the structure factor.

The DCS instrument was operated in the low resolution configuration using both 5 Å and 9 Å incoming neutron wavelength. In these configurations the instrumental energy resolution is a Gaussian function with a Full Width at Half Maximum (FWHM) of ≈ 100 μeV and ≈ 20 μeV, respectively. The highest Q available for the two configurations is ≈ 1.2 Å^{-1} and ≈ 2.0 Å^{-1}, respectively. A measurement of a standard vanadium sample was used to determine detector efficiency and the instrumental energy resolution. Static structure factors were obtained by integrating the scattered intensity from the ToF data collected using 5 Å incoming neutrons in the energy range from 2 meV to 1 meV.

Polarized diffraction measurements were performed with the NSE spectrometer using an incoming wavelength $\lambda = 5$ Å with $\Delta\lambda/\lambda \approx 20$ %. Dynamic NSE measurements, as it is well known[37,38], give results in the time domain. With the above defined configuration, the time range accessed by the instrument was from ≈ 3 ps to ≈ 8 ns. A measurement from a standard carbon sample was used to determine the instrumental resolution. In all cases, data were corrected for the scattering of the sample container, taking into account self-shielding effects through the samples' transmission, which was measured on DCS. Data were reduced and analyzed using routines available in DAVE[39].

2.3 Molecular Dynamics Simulation

To obtain further microscopic insight on structure and dynamics, we also performed MD simulations on mixtures of methanol and water molecules. In accordance with the experiments, we simulated four systems with the molar fraction of methanol molecules $x_M = 0.25$, 0.54, 0.75, and 1.0. For each system, totally 20000 molecules were first placed in a cubic box with periodic boundary conditions enforced in all directions and then equilibrated in the NPT ensemble at 1 bar and 298 K for 1 ns. By averaging the box size from the second half of this 1 ns equilibration period, we obtained and fixed the corrected box size for each system. The systems were equilibrated in the NVT ensemble at 298 K for another 1 ns before we collected trajectories. Finally, each system yielded a trajectory for 10 ns with a 0.1 ps interval in the NVT ensemble at 298 K.

All simulations were performed using GROMACS 5.0.7[40]. We utilized a leapfrog integrator with a time step of 1 fs. The OPLS-AA[41] force field with the TIP4P[42] water model was adopted to describe the interactions between methanol and water molecules. The geometric combination rule was applied to all the Lennard-Jones cross interactions. Bond lengths associated with hydrogen atoms were constrained to their equilibrium values using the LINCS[43] and SETTLE[44] algorithms for methanol and water molecules, respectively. The Lennard-Jones interactions were truncated at 1.2 nm and the electrostatic interaction was computed by the particle-mesh Ewald method[45] with a real-space cutoff of 1.2 nm. During the simulations, we employed the Nosé-Hoover thermostat[46–48] where the temperature coupling was enforced and the Berendsen barostat[49] where the pressure coupling was applied. The post-processing of the trajectories was performed using *LiquidLib*[50] to compute the structure factor and time correlation functions.

3 Theoretical Background

3.1 Neutron Scattering Measurements

In a dynamic neutron scattering experiment the relevant measured quantity is the dynamic structure factor, $S(Q,E)$, which is the sum of a coherent, $S_{coh}(Q,E)$, and incoherent, $S_{inc}(Q,E)$, term:[25,51]

$$S(Q,E) = S_{coh}(Q,E) + S_{inc}(Q,E)$$

where the wavevector (a scalar for amorphous samples) and energy transfer, $Q = |\mathbf{k}_i - \mathbf{k}_f|$ and $E = E_i - E_f$, respectively, are defined by the differences between the initial and final wavevector, $\mathbf{k_i}$ and $\mathbf{k_f}$, and energy of the neutrons, E_i and E_f. The integral of the dynamics structure factor over all energies is the static structure factor: $S(Q) = \int_{-\infty}^{\infty} S(Q,E)dE$.

The neutron coherent dynamic structure factor is defined as the sum of the dynamic structure factors of all pairs of atomic species α and β, as detailed in Section I of the SI. The weight of each partial structure factor is determined by the product of the coherent scattering lengths of the atoms in the pair, as well as by the number of such pairs present in the sample. The incoherent dynamic structure factor is similarly given by the sum of the incoherent

dynamic structure factor of each atomic specie, as also detailed in section I of the SI. The weight of each partial incoherent dynamic structure factor is determined by the incoherent scattering length density of the associated atom, as well as by its amount (number of atoms) in the sample.

In general, the coherent and incoherent dynamic structure factors are defined as the Fourier transform of the coherent and incoherent intermediate scattering functions, $I_{coh}(Q,t)$ and $I_{inc}(Q,t)$, respectively:

$$\begin{aligned} S_{coh}(Q,E) &= \mathcal{F}\{I_{coh}(Q,t)\} \\ S_{inc}(Q,E) &= \mathcal{F}\{I_{inc}(Q,t)\} \end{aligned}$$

In methanol/water mixtures, the three hydrogen atoms of the methanol methyl group are equivalent as are the two hydrogen atoms of the water molecule; therefore, fifteen partial structure factors, $S^{\alpha\beta}(Q,E)$, can be defined. In the four samples investigated the coherent scattering is a weighted sum of these fifteen partial structure factors, where the weights will depend on the deuteration scheme. In fact, the coherent scattering length and the incoherent scattering cross section of H and D are different. In all samples a non negligible contribution from the incoherent scattering is present. In order to gain deeper insight, the following procedure has been adopted which eliminates the incoherent scattering contribution and reduces the number of atomic correlations contributing to the signal. Similarly to what was previously done for methanol[29] and dodecanol[31], the following combination of the dynamic structure factors (denoted by a superscript "C", indicating combination) arising from the four samples investigated was calculated:

$$\begin{aligned} S^C(Q,E) =& S^{S1}(Q,E) + S^{S4}(Q,E) - \left[S^{S2}(Q,E) + S^{S3}(Q,E)\right] \\ =& \frac{2}{N_M^a x_M + N_W^a(1-x_M)}\sqrt{n_{M_M}}(b_D^{coh} - b_H^{coh})^2 \cdot \\ & \left[\sqrt{n_{M_H} x_M^2} S_{coh}^{MM-MH}(Q,E) + \right. \\ & \left. \sqrt{n_{W_H} x_M (1-x_M)} S_{coh}^{MM-WH}(Q,E)\right] \end{aligned} \tag{1}$$

where i) $S^{Sx}(Q,E)$ is the dynamic structure factor of sample Sx (x being 1|2|3|4); ii) x_M is the methanol mole fraction; iii) b_D^{coh} and b_H^{coh} are the coherent scattering lengths of D and H, respectively;[51] iv) $N_M^a = 6$ and $N_W^a = 3$ are the number of atoms in each methanol and water molecule, respectively; and v) $n_{M_M} = 3$ is the number of hydrogen atoms in the methyl group of methanol, $n_{M_H} = 1$ is the number of hydrogen atoms in the hydroxyl group of methanol, and $n_{W_H} = 2$ is the number of hydrogen atoms in the water molecule.

$S_{coh}^{MM-MH}(Q,E)$ and $S_{coh}^{MM-WH}(Q,E)$ are the partial dynamic structure factors corresponding to the relative motion of the hydrogens of the methyl group of methanol with respect to the hydrogens in the hydroxyl group of methanol and water, respectively. The aggregated atom content of samples S1 and S4 is the same as that of samples S2 and S3, which implies that the neutron incoherent scattering is the same for the two couples of samples in the aggregate. On the other hand, the contribution of the coherent partial dynamic structure factors $S_{coh}^{MM-MH}(Q,E)$ and $S_{coh}^{MM-WH}(Q,E)$ is weighted differently in the four samples, because of their different isotopic composition;* at the same time, all other partial coherent dynamic structure factors are weighted equally. Therefore, in conclusion, in Eq. 1 the incoherent scattering terms as well as most of the coherent partial structure factors cancel each other, so that $S^C(Q,E)$ does not contain any incoherent scattering contribution and is the sum of just two partial dynamics structure factors, hence it gives information on the correlation between three specific atomic groups in the system, only.

In the SI, a discussion of the uncertainties related to the use of the isotopic substitution method outlined above is carried out in Section II.

In the time domain, an ISF, $I^C(Q,t)$, containing the same information as $S^C(Q,E)$ can be defined through the relation:

$$\begin{aligned} S^C(Q,E) =& \frac{2\sqrt{n_{M_M}}(b_D^{coh} - b_H^{coh})^2}{N_M^a x_M + N_W^a(1-x_M)} \cdot \\ & \mathcal{F}\left\{\sqrt{n_{M_M} x_M^2} I_{coh}^{MM-MH}(Q,t) + \right. \\ & \left. \sqrt{n_{W_H} x_M (1-x_M)} I_{coh}^{MM-WH}(Q,t)\right\} \\ =& \mathcal{F}\left\{I^C(Q,t)\right\} \end{aligned} \tag{2}$$

It is common practice when performing Small Angle Neutron Scattering (SANS) experiments to report static scattering curves as normalized by the scattering volume rather than by the total number of atoms. The atom number density n^A, the number of atoms per unit volume, provides the appropriate conversion factor:

$$\hat{S}(Q,E) = n^A S(Q,E) \tag{3}$$

$$\hat{S}^C(Q,E) = n^A S^C(Q,E) \tag{4}$$

3.1.1 Polarized neutron diffraction and NSE measurements

Using a polarized neutron beam to perform a diffraction measurement, NSE allows the separation of the coherent and incoherent contribution to the scattering[52].

As far as the dynamic NSE measurements are concerned, the measured quantity is the normalized ISF, where coherent and incoherent contribution are weighted by the probability of the scattered neutron to have its spin flipped:

$$\frac{I_{NSE}(Q,t)}{I_{NSE}(Q,0)} = \frac{I_{coh}(Q,t) - \frac{1}{3}I_{inc}(Q,t)}{I_{coh}(Q,0) - \frac{1}{3}I_{inc}(Q,0)}$$

where $I(Q,0) = I(Q,t=0) = S(Q)$.

* The contribution of the partial coherent dynamic structure factors $S_{coh}^{MM-MH}(Q,E)$ and $S_{coh}^{MM-WH}(Q,E)$ will be weighted by $(b_D^{coh})^2$ in sample S1, by $(b_H^{coh})^2$ in sample S4, and by $b_D^{coh} b_H^{coh}$ in sample S2 and S3.

In the present paper, only NSE data obtained from the combination of samples S1-S4 according to equation 2 will be reported. As mentioned above, in this case the incoherent scattering is null and hence the normalized ISF measured by NSE coincides, apart from a scaling factor, with the Fourier transform of the data measured on DCS. For this reason, in the remainder of the paper, the subscript NSE will be omitted.

4 Results and discussion

4.1 Structure

Static structure factor measurements, as carried out on SANS and SPINS, provide information on the molecular arrangement at the nanoscopic scale.

Figure 1 a) reports the data collected using SANS on the four samples investigated. The scattered intensity in the low Q region (Q<0.6 Å^{-1}) is flat indicating no obvious presence of inhomogeneities at the Å to nm length scale. The scattering intensity of the four samples scales with the hydrogen content of the samples, which confirms that for samples S2-S4 most of the scattering is incoherent. However, it should be mentioned that for Q values less than ≈ 1 Å^{-1}, polarized diffraction measurements from NSE, which will be discussed later, indicate that even for the perdeuterated sample, S1, about 2/3 of the scattering intensity is incoherent. As mentioned above, for each S1-S4 sample three specimens have been prepared for the SANS measurements. The three sets of data are combined to obtain an 'averaged' scattering pattern for each sample to minimize the uncertainty in the sample amount.

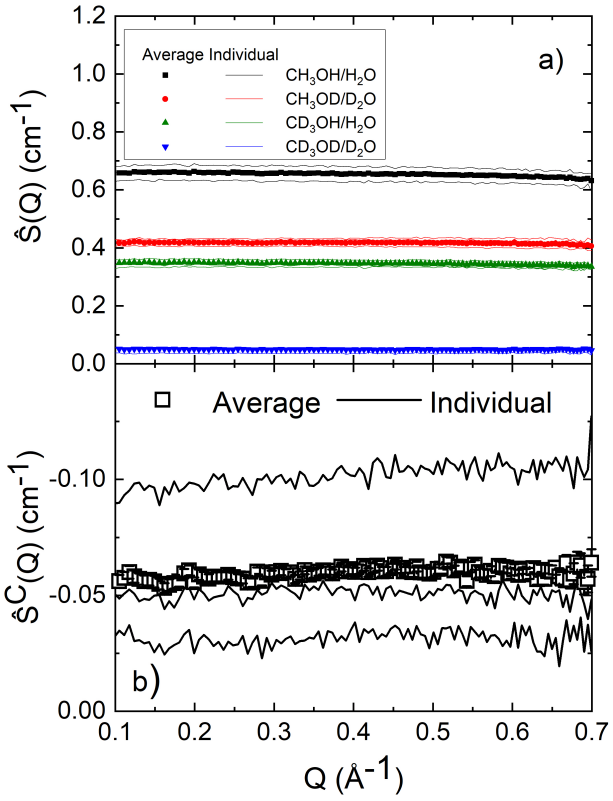

Fig. 1 a) The static structure factor measured for S1-S4 samples using SANS. For each sample three sets of data (individual) were collected using different specimens for the measurements. The three sets of data give an indication of the reproducibility with respect to the sample thickness. The points represent the average of the sum of the three samples. The statistical error of the measurement is smaller than the symbol size. Please, note that in some cases the average data overlap with one of the individual data sets, which is then not visible. b) $\hat{S}^C(Q)$ as determined by SANS at room temperature. Three measurements were performed on three set of samples, indicated by lines; the symbol represent the averaged result.

The SANS data have been combined to calculate $\hat{S}^C(Q)$ using Eq. 1. These data should be considered a sensitive measurement of the methyl groups arrangement with respect to the water molecules and the hydroxyl groups of methanol. The results are reported in Fig. 1 b). No obvious signature of structuring is observed. Again data are reported for the combination of the three individual specimens tested and for their average.

Remarkably, $\hat{S}^C(Q)$ is negative. This would not be possible for an experimentally measured structure factor but it is for a partial structure factor, whose asymptotic high-Q value is zero.

The investigation of the structure factor to larger Q values, and therefore smaller length scales, has been carried out using NSE, SPINS, and DCS.

Fig. 2 reports $\hat{S}^C(Q)$ up to 2.5 Å^{-1}. To obtain these results in absolute intensity, data have been scaled to agree with the SANS results as exemplified in Fig. S1 of the SI.

Fig. 2 a) reports the polarized diffraction data obtained using NSE at $T = 200$ K. These data validate that the isotopic substitution procedure employed is able to cancel out the incoherent scattering which is zero within experimental uncertainties. It is worth noting that from the polarization analysis, the coherent scattering is dominant only in the perdeuterated sample and only at the FSDP, which justify the need for the isotopic substitution method employed here to extract the information on the collective dynamics.

Fig. 2 panels b) and c) show the behavior of $\hat{S}^C(Q)$ in the extended Q range probed by SPINS and DCS, respectively, at four temperatures in the range from 290 K to 200 K. The agreement between the results obtained with the two spectrometers is satisfactory. The flat negative region measured by SANS extends from low-Q up to almost 1.5 Å^{-1}. After that, $\hat{S}^C(Q)$ increases, becoming positive, reaching a maximum at ≈ 1.8 Å^{-1}. Hence, for both $\hat{S}(Q)$ of the perdeuterated sample (see SI Fig. S2) and $\hat{S}^C(Q)$ the position of the FSDP is the same at ≈1.8 Å^{-1}. However, $\hat{S}^C(Q)$ peak is broader and more asymmetric with a tail towards high Q values which extend beyond the Q values accessed here.

To make a comparison to previous results based on thermodynamic parameters as well as to allow for a comparison to binary liquid mixture models, we employ the approximation that the internal molecular structure of methanol and water can be ignored and that internal parameters such as orientation and molecular conformation can be neglected; it follows that:

$$S_{coh}^{MM-WH}(Q,E) \approx \sqrt{n_{M_M} n_{W_H}} S_{coh}^{CM_M-CM_W}(Q,E)$$

$$S_{coh}^{MM-MH}(Q,E) \approx \sqrt{n_{M_M} n_{M_H}} S_{coh}^{CM_M-CM_M}(Q,E)$$

where CM_M and CM_W indicate the center of mass of the

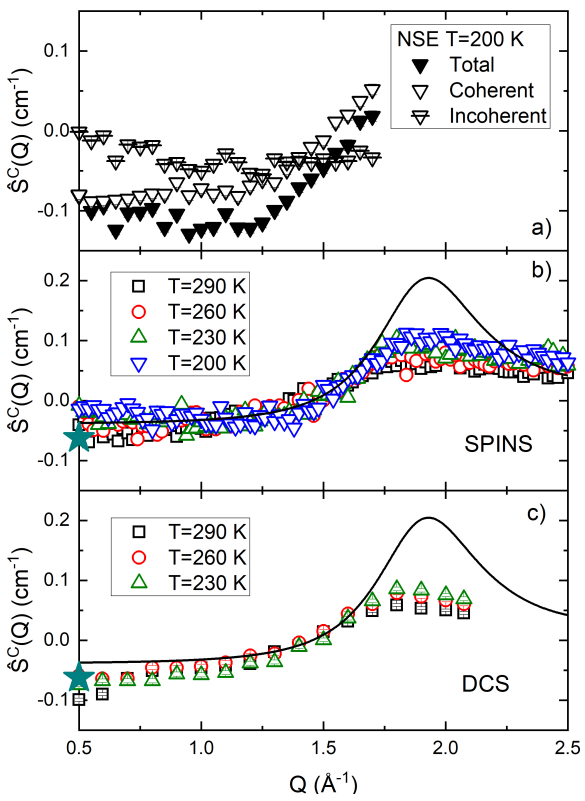

Fig. 2 The combined scattering intensity of S1-S4 according to equation 1, $\hat{S}^C(Q)$, as obtained on different instruments, at different temperatures. a) $\hat{S}^C(Q)$, as determined using NSE at T=200 K and its decomposition in a coherent and incoherent (negligible) contributions, through polarization analysis. b) SPINS results. c) DCS results. In b) and c) the continuous line represent the distinct term of the structure factor for binary hard spheres.

methanol and water molecules, respectively. There follows an approximate expression for $S^C(Q,E)$:

$$\begin{aligned} S^C(Q,E) \approx & S_a^C(Q,E) \\ = & \frac{2}{N_M^a x_M + N_W^a (1-x_M)} n_{M_M} (b_D^{coh} - b_H^{coh})^2 \cdot \\ & \Big[n_{M_H} x_M S_{coh}^{CM_M - CM_M}(Q,E) + \\ & n_{W_H} \sqrt{x_M (1-x_M)} S_{coh}^{CM_M - CM_W}(Q,E) \Big] \end{aligned} \tag{5}$$

and

$$\begin{aligned} \hat{S}_a^C(Q,E) = & n^A S_a^C(Q,E) \\ = & 2 n^{mol} n_{M_M} (b_D^{coh} - b_H^{coh})^2 \cdot \\ & \Big[n_{M_H} x_M S_{coh}^{CM_M - CM_M}(Q,E) + \\ & n_{W_H} \sqrt{x_M (1-x_M)} S_{coh}^{CM_M - CM_W}(Q,E) \Big] \end{aligned} \tag{6}$$

with n^{mol} molecule number density.

The above expression are expected to be valid at large length scales, i.e. for small Q such that $\mathbf{Q}(\mathbf{r}_{i_M}^{CM} - \mathbf{r}_{i_{MM}}) \ll 1$.

For binary liquid mixtures, scattering originates from fluctuations of concentration and density, as well as their cross-correlations; however, the cross terms partial structure factor is known to be mostly determined by the concentration fluctuations. In the thermodynamic limit, i.e. for $Q \to 0$, the static variable can be related to thermodynamic quantities, such us the isothermal compressibility, the molar volumetric properties and the chemical potential, using the Kirkwood-Buff integrals:

$$\begin{aligned} S_{coh}^{CM_M - CM_W}(Q \approx 0) = & \frac{1}{\sqrt{N_M N_W}} \sum_{i_M=1}^{N_M} \sum_{i_W=1}^{N_W} \langle e^{i\mathbf{Q}\cdot\left[\mathbf{r}_{i_M}^{CM}(0) - \mathbf{r}_{i_W}^{CM}(0)\right]} \rangle \\ = & \sqrt{\rho_M^{mol} \rho_W^{mol}} G_{MW} \end{aligned} \tag{7}$$

$$\begin{aligned} S_{coh}^{CM_M - CM_M}(Q) = & \frac{1}{N_M} \sum_{i_M=1}^{N_M} \sum_{i_M=1}^{N_M} \langle e^{i\mathbf{Q}\cdot\left[\mathbf{r}_{i_M}^{CM}(0) - \mathbf{r}_{i_M}^{CM}(0)\right]} \rangle \\ = & \{1 + \rho_M^{mol} G_{MM}\} \end{aligned} \tag{8}$$

where ρ_M^{mol} and ρ_W^{mol} are the methanol and water molecules number density, respectively, and G_{MM} and G_{MW} are the methanol-methanol and methanol-water Kirkwood-Buff integrals, respectively[53]. The cyan stars in Fig. 2, indicates the value of $\hat{S}^C$(Q→0) calculated from the known values of the Kirkwood-Buff integrals.[54] The agreement between the experimental and calculated result provides strong support of the validity of the employed experimental method.

Furthermore, using Eq. 5, in a broader Q range, $\hat{S}^C(Q)$ can be compared with the calculations for the model system of a mixture of hard spheres of two different sizes.[55] The parameters required for the calculation, namely the fraction of the volume occupied by the spheres, $\eta_S \approx 0.22$, and the ratio of the radius of the spheres, $\alpha = 0.8$, were determined using the known density values of methanol/water mixtures, the radius of the water molecule, $R_W = 3$ Å, and by having a $Q \to 0$ value of the three partial structure factors best approximating the known Kirkwood-Buff integrals. The results of the calculation are reported in Fig. 2 as a continuous black line. The qualitative behavior of $\hat{S}^C(Q)$ is well reproduced with an initial plateau level with a negative value followed by a peak at a Q value intermediate between the structure factor peaks of the pure components, 1.75 Å^{-1} and 1.95 Å^{-1} for methanol and water respectively.[28,56] The low and intermediate Q range (Q<1.5 Å^{-1}) behavior is quantitatively in agreement with the hard spheres mixture model prediction, notwithstanding that the model is an oversimplification for associating liquids such as methanol and water. This is remarkable also in the context of the phenomenon of microsegregation in methanol/water and alcohol/water mixtures in general. Perera and co-workers[12] suggest that whereas concentration fluctuations produce an increase of the low-Q scattering which is reflected by the Kirkwood-Buff integral values, micro-segregation and association is signaled by the presence of a pre-peak. In fact in a previous work on methanol, employing a similar isotopic substitution method as the one employed here, some of the authors were able to experimentally observe a prepeak in methanol at $Q \approx 1.1$ Å^{-1}.[29]

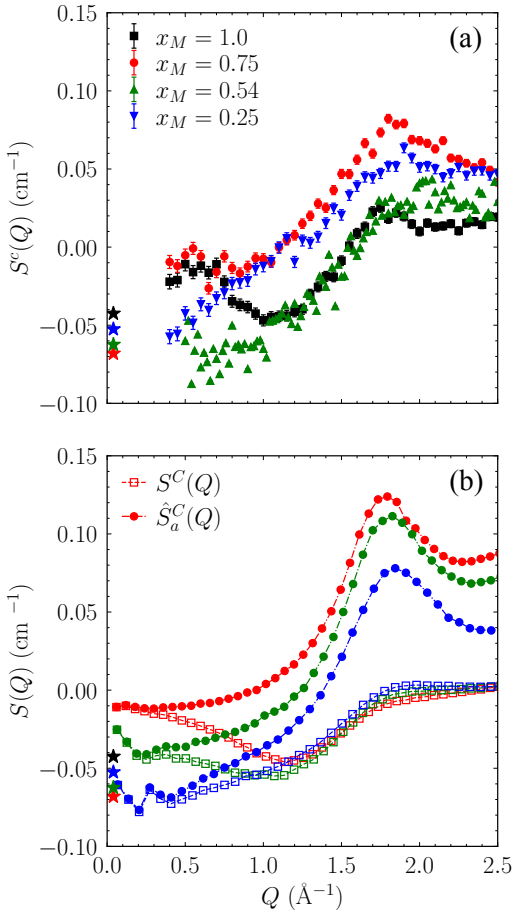

Fig. 3 (a) The combined scattering intensity of S1-S4 according to equation 1, as obtained on SPINS for various methanol/water mole fractions. (b) The simulation structure factor of $\hat{S}^C(Q)$ and $\hat{S}_a^C(Q)$. The Kirkwood-Buff integrals of each sample are indicated by the stars at $Q = 0$ in both figures.

To the best of our knowledge, a similar finding was never reported for water, notwithstanding that it is accepted that water forms an extensive hydrogen bond associating network. As far as the methanol/water mixtures are concerned, a prepeak in the oxygen-oxygen correlation function was reported from MD simulation.[8] However, experimentally, no such feature could be observed here, putting further in evidence how it can be difficult to experimentally find direct evidence of microsegregation and association through the investigation of the static structure factor, alone.

An analysis of the concentration dependence of the dynamics in the methanol water system is beyond the focus of this paper. However, Fig. 3 reports the comparison between the behavior of $\hat{S}^C(Q)$ at different methanol/water molar fractions at room temperature. In pure methanol, as mentioned above, a previously reported[29] pre-peak at $Q \approx 1.1$ Å^{-1} is observed. However, at low water content (pure methanol and $x_M = 0.75$), there is little intensity in $\hat{S}^C(Q)$ at low Q. $\hat{S}^C(Q)$ takes non-null values for $x_M = 0.25$ and 0.54. This result correlates with the concentration dependence of the thermodynamic anomalies, i.e. excess enthalpy, entropy, and Gibbs free energy, which show extrema in the range between $x_M \approx 0.2$ and $x_M \approx 0.6$.[57] In particular, the excess molar Gibbs free energy has a maximum around the equimolar concentration, close to where the strongest low Q signal in $\hat{S}^C(Q)$ is observed. On the other hand, the agreement with $\hat{S}^C(Q \to 0)$ from the Kirkwood-Buff integrals is only fair; good quantitative agreement is observed at $x_M = 0.25$ and 0.54; however, for $x_M = 0.75$ and 1.0 the calculated value is lower than observed, especially for $x_M = 0.75$.

As observed in Fig. 2 the binary hard sphere model grossly fails to reproduce the data above ≈ 1.5 Å^{-1}. MD simulation can provide indications whether the internal molecular structure of methanol and water has a significant effect. MD simulations results for $\hat{S}^C(Q)$ are shown in panel b) of Fig. 3; calculations considering the atomic scattering, $\hat{S}^C$, or the center of mass of the molecules only, $\hat{S}_a^C$, are displayed. The values of the Kirkwood-Buff are reproduced with moderate accuracy. Interestingly, MD calculations for $\hat{S}^C$ yield a pre-peak at ≈ 1 Å^{-1}. This pre-peak has been observed both experimentally[29] (see also Fig. 3 a), $x_M = 1.0$) and from MD simulation[58] in bulk methanol, but it does not appear at intermediate methanol content in the experimental data shown in Fig. 3 a). This discrepancy cautions against solely relying on MD results to validate the existence of microsegregation. $\hat{S}_a^C$ better reproduces the experimental data up to the structure factor peak, whose intensity is over-estimated, similarly to what seen for the mixture of two hard spheres model. Experimental data in the Q region around the structure factor peak are in between $\hat{S}^C$ and $\hat{S}_a^C$ from MD simulations. This result indicates that the present MD simulation do not precisely capture the properties of the methanol/water mixtures; however, the MD trajectories point to the fact that in the low and intermediate Q range $\hat{S}_a^C$ approximate the experimental results with sufficient accuracy.

4.2 Dynamics

4.2.1 Dynamics in the hydrodynamic limit: Mutual diffusion

We now turn the focus on the molecular dynamics of the mathanol/water mixtures. As mentioned above regarding the partial static structure factors, within a formalism introduced by Bhatia and Thornton[59], the partial dynamic structure factors of a binary mixture can be expressed in terms of a concentration, $S_{xx}(Q,E)$, number density, $S_{nn}(Q,E)$, as well as cross term, $S_{nx}(Q,E)$, dynamic structure factors or, equivalently by the corresponding intermediate scattering functions, $I_{xx}(Q,t)$, $I_{nn}(Q,t)$, and $I_{nx}(Q,t)$. Thus:

$$\begin{aligned} I^{CM_M-CM_M}(Q,t) =& I_{xx}(Q,t) + 2x_M I_{nx}(Q,t) + x_M^2 I_{nn}(Q,t) \\ I^{CM_M-CM_W}(Q,t) =& -I_{xx}(Q,t) + (1-2x_M) I_{nx}(Q,t) - \\ & x_M(1-x_M) I_{nn}(Q,t) \end{aligned} \quad (9)$$

The hydrodynamic limit of these functions have been calcu-

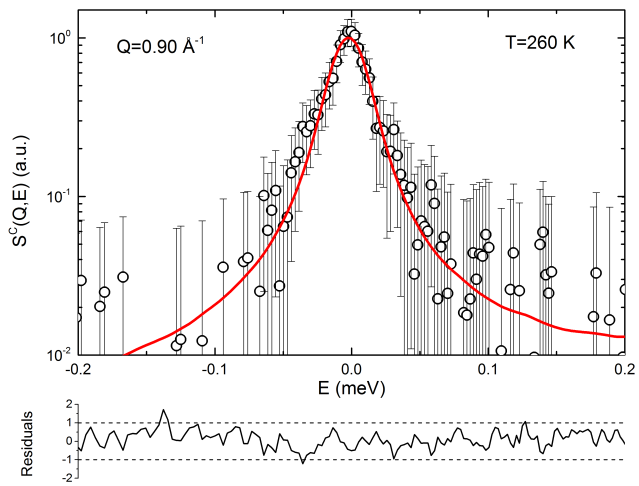

Fig. 4 Fitting of $S^C(Q,E)$ in terms of a Lorentzian function convoluted with the experimental resolution (see Eq. 11). Panel b) reports the residuals normalized to the experimental error, which, being mostly smaller than 1 in absolute value, confirm that the employed fitting model is able to satisfactorily reproduce the experimental data.

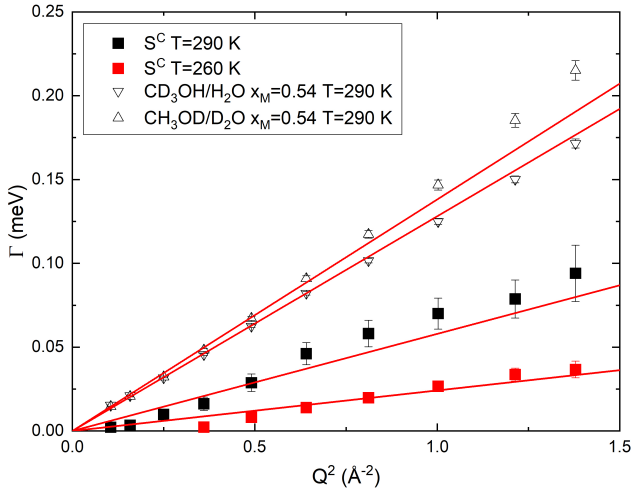

Fig. 5 The obtained values of Γ as a function of Q^2. Solid data points refer to the fitting of $S^C(Q,E)$ at 290 K and 260 K. Open up and down triangles are the results for the CH_3OD/D_2O and CD_3OH/H_2O at $x_M = 0.54$ samples, respectively. The data are analyzed according to a diffusion model with a straight line (Eq. 12).

lated resulting in the sum of two exponential decays[60] with relaxation rates determined by the thermal diffusivity and the mutual diffusion, as detailed in section III of the SI.

For methanol/water mixtures at 290 K, the thermal diffusivity can be estimated[61–63] to be of the order of 10^{-7} m^2/s, which is too fast to be measured within the experimental window. Moreover, with reference to Eqs. S7, the weight of its contribution is about two orders of magnitude smaller that the one associated with the mutual diffusion.[64,65] It results that in the relevant time window the dynamics probed is the mutual diffusion:

$$I^{CM_M-CM_M}(Q\to 0,t) \approx \exp\left[-D^M Q^2 t\right]$$
$$I^{CM_M-CM_W}(Q\to 0,t) \approx \exp\left[-D^M Q^2 t\right] \quad (10)$$

On the basis of the analysis above, the relative motion of the water to methanol molecules can be investigated through the study of the $S^C(Q,E)$ data. Previous investigation of the coherent quasielastic broadening in methanol/water mixtures were performed only using light scattering techniques;[66] therefore were limited to the hydrodynamic limit. The hydrogen bonding dynamics was investigated using depolarized Rayleigh scattering[67] identifying a maximum in the hydrogen bonding relaxation time at equimolar concentration. The QENS $S^C(Q,E)$ data represent, to the best of our knowledge, the first nanoscopic scattering investigation of the mutual molecular dynamics in methanol/water mixtures.

The QENS spectra can be analyzed in terms of a Lorentzian function convoluted with the experimentally determined resolution, $R(Q,E)$, function:

$$\frac{S^C(Q,E)}{S^C(Q)} = \frac{A(Q)}{\pi}\frac{\Gamma(Q)/2}{E^2+\left[\frac{\Gamma(Q)}{2}\right]^2} \otimes R(Q,E) \quad (11)$$

where A(Q) is a Q dependent amplitude factor and Γ(Q) is the Full Width at Half Maximum (FWHM).

Fig. 4 reports an example of the fitting of $S^C(Q,E)$.

Fig. 5 reports the Q^2 dependence of the parameter Γ as obtained from the fits of the S^C data collected using 9 Å neutrons. DCS results from different incoming wavelength agree well with each other. Fig. 5 also reports the results obtained from the analysis of the data collected on CD_3OH/H_2O and CH_3OD/D_2O at $x_M = 0.54$, using Eq. 11. In these latter cases the single particle dynamics of the hydrogen atoms in the methyl or hydroxyl groups and water is observed. The obtained results compare well with previously published results of the single particle hydrogen dynamics in similar systems.[26,68] The collective dynamics associated with the methyl to hydroxyl and water correlation, as measured from S^C, is significantly slower than the single particle dynamics of the hydrogen in the system. This is a clear indication of correlated motion of the methyl vs hydroxyl groups.

As shown in Fig. 5, the Γ values scale with Q^2 within experimental uncertainties which can usually be associated with a diffusive behavior. Based on the comparison with Eq. 10, a mutual diffusion coefficient at the nanoscopic level D_n^M can thus be extracted:

$$\Gamma = 2D_{\rm n}^{\rm M}Q^2 \quad (12)$$

In order to extend the temperature range investigated, $I^C(Q,t)/I^C(Q,0)$, the normalized intermediate scattering function corresponding to $S^C(Q,E)/S^C(Q)$, at 200 K and $Q = 0.31$ Å^{-1} was measured using NSE. The obtained results are shown in Fig. 6. The data can be analyzed in terms of a simple exponential relaxation in agreement with the analysis of $S^C(Q,E)$ using a Lorentzian function.

Fig. 7 is an Arrhenius plot of the comparison between D_n^M and reported macroscopic self and mutual (binary) diffusion coefficients of methanol and water.[69]

The self diffusion of methanol and water molecules exceeds the mutual diffusion and D_n^M, indicating a slower relative dynamics

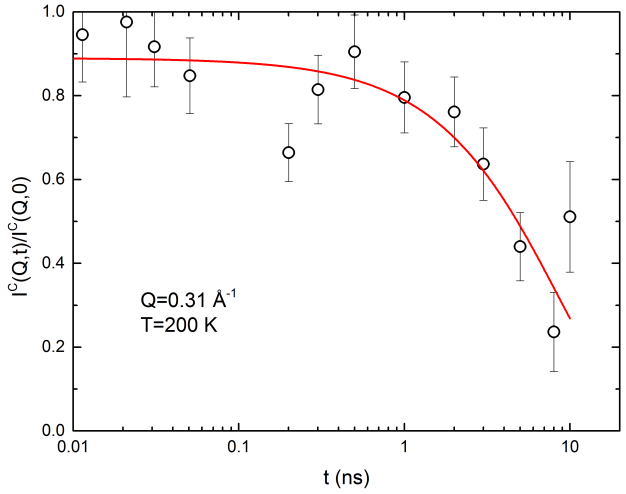

Fig. 6 Normalized intermediate scattering function as obtained from the NSE measurements. The data are fitted with an exponential decay.

Table 1 Diffusion coefficients (Å^2/ps) as obtained from the MD simulations of methanol/water with $x_M = 0.54$.

Diffusion coefficients	
$D^{\mathrm{M}}_{\mathrm{self}}$	0.225 ± 0.003
$D^{\mathrm{W}}_{\mathrm{self}}$	0.220 ± 0.002
$D^{\mathrm{CM_M - CM_W}}$	0.185 ± 0.004
D^{SC}_{MD}	0.197 ± 0.002
D^{M}_{MD}	0.102 ± 0.001

of the two molecular species. In harmony with the discussion above, the existence of association between methanol and water molecules explains the slowing down of the mutual nanoscale motion of the two molecular species. In particular, the fact that the relative diffusion at the molecular level, as determined from D^M_n, is about a factor of three slower than the macroscopic mutual diffusion coefficient is a direct indication of association. In fact, the observation of a nanoscopic relaxation dynamics slower than the hydrodynamic extrapolated behavior in methanol has been indicated as a signature of the presence of molecular associates.[28]

MD results support this scenario. The mutual diffusion coefficient was determined following Zhou and Miller,[70] as (see Fig. S3 in the SI):

$$D^M_{MD} = \frac{A}{N x_M (1 - x_M)} \lim_{t\to\infty} \frac{\langle |\mathbf{r}_{12}(t) - \mathbf{r}_{12}(0)|^2 \rangle}{6t} \qquad (13)$$

where

$$\mathbf{r}_{12}(t) = (1 - x_M) \sum_{i=1}^{N_M} \mathbf{r}_i^{CM_M}(t) - x_M \sum_{j=1}^{N_W} \mathbf{r}_j^{CM_W}(t) \qquad (14)$$

$\mathbf{r}_i^{CM_M}$ and $\mathbf{r}_j^{CM_W}$ being the position of the center of mass of the i-th methanol molecule and j-th water molecule, respectively, and

$$A = \frac{1}{1 + \rho x_M (1 - x_M)(\Gamma_{MM} + \Gamma_{WW} - 2\Gamma_{MW})} \qquad (15)$$

where ρ is the molecular number density and $\Gamma_{ij} = 4\pi \int_0^\infty r^2 [g_{ij}(r) - 1] dr$ is the Kirkwood-Buff integral. During the calculation of Kirkwood-Buff integrals, a cutoff distance of 18 Å was selected as integration values become stable, as previously indicated.[8]

The single particle ISFs of water and methanol in the mixture, as well as $I^{CM_M - CM_W}$ and I^C were calculated from the MD trajectories. The corresponding diffusion coefficients, D^M_{self}, D^W_{self}, $D^{\mathrm{CM_M - CM_W}}$ and D^{SC}_{MD}, respectively, were determined from the Q dependence of the decay to $1/e$ of the ISF (see Fig. S3 in the SI). Table 1 summarizes the obtained results. The qualitative trend agrees with the experiments: both the mutual and effective diffusion coefficients are slower than the single particle ones indicating the presence of association among unlike species in clusters.

A recent study suggests that the standard geometric combination rule for the interaction between the methanol and water oxygen sites may not be able to capture the excess excess enthalpy of the system accurately[71]. A specific parameterization can be applied to appropriately reproduce the excess of thermodynamics of short-chain alcohol/water system[71]. In this work, the excess enthalpy of methanol/water mixture could be overestimated by simulation, which may lead to obtaining a slower mutual dynamics. On the other hand, the experienced combination rule is also widely used in simulating alcohol/water mixtures[8,72,73] and our simulations compare well with the neutron scattering results. Therefore, we believe that the effect of excess enthalpy will not significantly influence our conclusions.

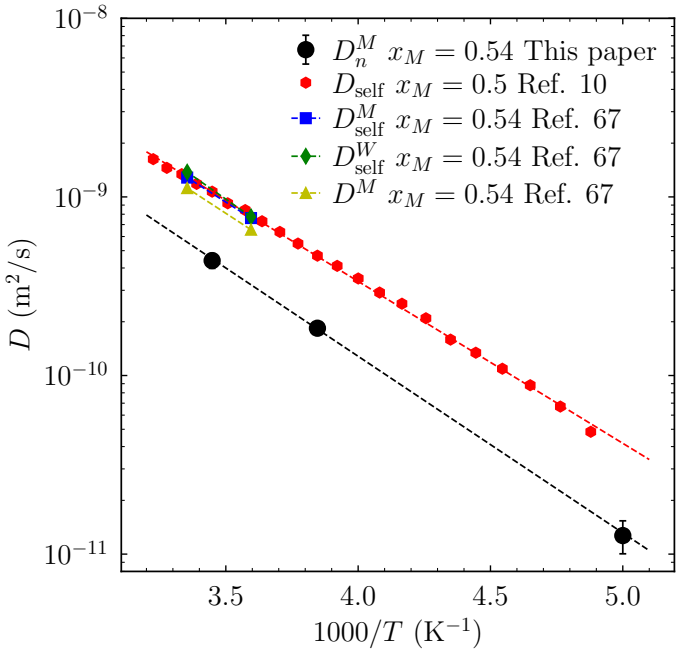

Fig. 7 Arrhenius plot of the nanoscopic mutual diffusion coefficient, D^M_n, with previous reports of the self diffusion coefficient of methanol/water mixtures at $x_M = 0.5$ by NMR,[10] (red circles) and of the self diffusion coefficients of methanol (blue squares) and water (green diamonds) in the mixture, as well as of the mutual diffusion coefficient (dark yellow triangles) obtained by tracer diffusion.[69]

4.2.2 Structural relaxation

As mentioned above, another unusual phenomenon observed in methanol/water mixture is the fact that its viscosity reaches a maximum at $x_M \approx 0.25$, taking a value larger than that of both pure water and pure methanol.[74] Similar behavior is observed in other mixtures of water with alcohols and it has been thought to originate from microsegregation.[75,76]

At the structure factor peak, the coherent scattering signal is commonly related to the structural relaxation of the system, the molecular motion over intermolecular distances representing the fundamental relaxation process in liquids,[77] and the thus determined relaxation time is identified with the structural relaxation time, τ_R, and the Maxwell relaxation time, τ_{Maxwell}. This latter provides a connection with the macroscopic viscosity, η, being defined as: $\tau_{\mathrm{Maxwell}} = \eta/G_\infty$; where G_∞ is the shear modulus at infinite frequency. The relation between the macroscopic viscosity and the molecular structure and dynamics is complex; however, the comparison between the structural relaxation time and viscosity provides insights into the role played by molecular association and the structural relaxation.[78] In the past, the relevance of hydrogen bonded associates in determining the macroscopic viscosity has also been shown in methanol, dodecanol and isopropanol.[31,76,79] In particular, using selective deuteration methods, similar to the one employed here, it has been possible to highlight the coincidence of the temperature dependence of the viscosity with that of the dynamics of specific molecular associates, which demonstrate their role in determining macroscopic transport properties.

In order to compare the timescale of the lifetime of the methanol/water associates with the structural relaxation, both the $S^C(Q,E)$ and the perdeuterated $S^{S1}(Q,E)$ data at $Q = 1.8$ Å^{-1}, in correspondence to the FSDP, were analyzed. The $S^C(Q = 1.8\ \text{Å}^{-1}, E)$ data could be fitted according to Eq. 11 (see Fig. S4 in the SI). In the perdeuterated sample case, two Lorentzian functions were required for a satisfactory fit (See Fig. S5 in the SI):

$$S^{S1}(Q,E) = \frac{A(Q)}{\pi}\left\{ A_1(Q)\frac{\Gamma^{S1}(Q)}{E^2 + \left[\frac{\Gamma(Q)}{2}\right]^2} + [1 - A_1(Q)]\frac{\Gamma_1^{S1}(Q)}{E^2 + \left[\frac{\Gamma_1(Q)}{2}\right]^2}\right\} \otimes R(Q,E) \quad (16)$$

The fact that a simpler model is sufficient to analyze the $S^C(Q,E)$ data could originate from the fact that only 2 partial dynamic structure factors contribute to $S^C(Q,E)$ but it could also be a mere consequence of the lower statistical quality of the data.

Both the $S^C(Q,E)$ and $S^{\mathrm{S1}}(Q,E)$ data could be analyzed in the temperature range from 290 K to 230 K. As far as the perdeuterated sample is concerned, the broader Lorentzian component is temperature independent with a FWHM $\Gamma_1^{S1} \approx 2$ meV, corresponding to a dynamics on the time scale of the fraction of 1 ps. The total spectral intensity, $A(Q)$, is also temperature independent, whereas, the spectral weight of the slow component, A_1, increases with decreasing temperature from 0.43 ± 0.03 at 290 K to 0.64 ± 0.03 at 230 K. The fast relaxation can be attributed to rearrangements of the molecules without breaking of the first neighbors cage, as observed in 2-propanol.[76] For both samples, FWHM values obtained in correspondence of the FSDP were translated into a characteristic relaxation time:

$$\tau_R^C = \frac{2\hbar}{\Gamma} \quad (17)$$

$$\tau_R = \frac{2\hbar}{\Gamma^{S1}} \quad (18)$$

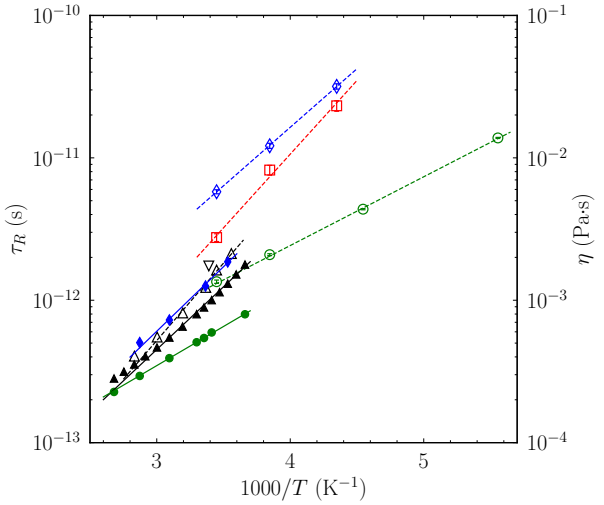

Fig. 8 Arrhenius plot of the relaxation time (hollow) and viscosity (solid). Black triangles represent values for water[80]; green circles represent values for methanol[29]; blue diamonds represent values for $x_M = 0.54$ methanol-water mixture (present work); red squares represent values for calculated S^C (present work). The corresponding activation energies are reported in Tab. 2.

Fig. 8 is an Arrhenius plot of structural relaxation in water, methanol, and methanol/water mixtures compared with the macroscopic shear viscosity. The viscosity of water does not follow an Arrhenius law; however, considering a relatively small temperature range around room temperature, an activation energy value can be extracted. Table 2 reports the values of the activation energies for the data shown in Fig. 8. The activation energies are $E_{\mathrm{a}}^{\tau_{\mathrm{R}}} = (15.7 \pm 0.1)$ kJ/mol for the perdeuterated sample at $Q = 1.8$ Å^{-1}, $E_{\mathrm{a}}^{\tau_{\mathrm{R}}^{\mathrm{C}}} = (19.9 \pm 1.6)$ kJ/mol for the S^C at $Q = 1.8$ Å^{-1}, whereas the activation energy for D^{M} was (18.9 ± 0.4) kJ/mol. Hence, the activation energy for the microscopic mutual diffusion process and for the structural relaxation of the associates are the same, indicating that the same microscopic process, i.e. the lifetime of the associates, triggers both motions. The values obtained for E_A lay in the range of hydrogen bond energy. However, in the sample investigated here the activation energy is much larger than for methanol, roughly by a factor of two, and close to the one of water. It is known that

methanol has a significant fraction of molecular associates, likely in the form of chains, however, also in water the H-bond network is ubiquitous with tetrameric and pentameric associates. Thus, in water more than one hydrogen bond has to be broken for the transport process to be triggered.[81] The obtained results indicate that this is the case also for methanol/water mixtures. The presence of methanol does not seem to enforce a chain like structuring in the system. In fact, structural x-ray investigations[13] find evidence that methanol chains coordinate with water trimers and tetramers.

Within a mode coupling theory approach, the dynamics at the structural peaks of a liquid largely determine its viscosity.[79,82] The activation energy for the viscosity, $\mathrm{E_a^{\eta}}$ is intermediate between $\mathrm{E_a^{\tau_R}}$ and $\mathrm{E_a^{\tau_R^C}}$. This finding, within the above mentioned approach, indicates that the atomic correlations probed by S^{C}, specifically the methanol water correlations, have a significant weight in determining the viscosity, even though other correlations play a role as well.

Within the approximation that the mutual relaxation time at the structure factor peak, τ_R^C, coincides with the Maxwell time, the data reported in Fig. 8 provide an estimate of the shear modulus at infinite frequency:

$$G_\infty^C = \frac{\eta}{\tau_M} \approx \frac{\eta}{\tau_R^C} \tag{19}$$

The obtained results are $G_\infty^W = 6.68 \times 10^8$ Pa, $G_\infty^C(x_M = 0.54) = (5.7 \pm 0.4) \times 10^8$ Pa, and $G_\infty^M = 4.64 \times 10^8$ Pa for water, methanol/water ($x_M = 0.54$), and methanol respectively. These values can be compared with an ideal behavior in which G_∞ can be obtained as the molar weighted sum of the methanol and water values: $x_M G_\infty^M + (1 - x_M) G_\infty^W = 5.58 \times 10^8$ Pa coincide, within experimental uncertainties with $G_\infty^C(x_M = 0.54)$. Even considering the employed approximations and experimental uncertainties, this results is a clear indication that the fact that the viscosity of methanol/water mixture, in a certain concentration range, is higher than the pure components originates from the molecular structuring and H-bonding, in particular between methanol and water nanoscopic associates.

5 Conclusions

Neutron scattering measurements employing a novel isotopic substitution technique provide new evidence of nanoscopic association among unlike molecular species in methanol/water mixtures. However, no indication of microsegregation was observed in the collected data. The associates are dynamical in character, their lifetime being determined by the diffusion of the water and methanol molecules; however, at the nanoscale the relative motion of the two molecular species with respect to each other is slowed down by association as compared to the single particle diffusion. This slow collective dynamic process is recognized as a signature of molecular association. The temperature dependence of the mutual dynamics matches that of the viscosity, a finding which highlights its role in determining the macroscopic transport properties. Estimating the value of the shear modulus at infinite frequency reveals that the fact that the viscosity of some methanol/water mixtures is higher than that of both pure component is related to the increase of the structural relaxation timescale. These results not only provide evidence of association in methanol/water mixtures but clarify how H-bonding affects the dynamics of the system and in turn the macroscopic transport properties. On the basis of these results, an analogous emergence of a slow mutual dynamics of the associates at the nanoscale is likely in other associating liquids with nanoscopic heterogeneities such as IL, DES, and WIS electrolytes, which might affects macroscopic transport properties relevant for their applications.

Table 2 Activation energy (kJ/mol) for the viscosity and the structural relaxation of methanol water mixtures.

x_M	η	τ_R	τ_R^C
0 (Water)[80]	16.9 ± 0.4	20.8 ± 1.0	
0.54	17.4 ± 0.1	15.7 ± 0.7	19.9 ± 1.6
1 (Methanol)[29]	10.5 ± 0.1	9.3 ± 0.1	

Disclaimer

The identification of any commercial product or trade name does not imply endorsement or recommendation by the National Institute of Standards and Technology. Uncertainties throughout this paper represent one standard deviation.

Conflicts of interest

There are no conflicts to declare.

Acknowledgements

The authors thank Dr. John Copley for assistance performing the QENS measurements on DCS. The authors are indebted to Dr. Chris Bertrand, Dr. Jose Teixeira, and Prof. Tsuyoshi Yamaguchi for helpful discussions. Access to the NSE spectrometer was provided by the Center for High Resolution Neutron Scattering, a partnership between the National Institute of Standards and Technology and the National Science Foundation under Agreement No. DMR-2010792. Support for Jackson Waller and Jeffrey Self was provided by the Center for High Resolution Neutron Scattering, a partnership between the National Institute of Standards and Technology and the National Science Foundation under Agreement No. DMR-2010792.

Data Availability

The data that support the findings of this study are available from the corresponding author upon reasonable request.

Notes and references

1 F. Franks and D. J. G. Ives, *Quarterly Reviews*, 1966, **20**, 1–+.
2 F. Franks, M. Pedley and D. S. Reid, *Journal of the Chemical Society-Faraday Transactions I*, 1976, **72**, 359–367.
3 A. H. Clark, F. Franks, M. D. Pedley and D. S. Reid, *Journal of the Chemical Society-Faraday Transactions I*, 1977, **73**, 290–305.
4 A. K. Soper and J. L. Finney, *Physical Review Letters*, 1993, **71**, 4346–4349.
5 S. Dixit, J. Crain, W. C. K. Poon, J. L. Finney and A. K. Soper, *Nature*, 2002, **416**, 829–832.

6 G. Darrigo and J. Teixeira, *Journal of the Chemical Society-Faraday Transactions*, 1990, **86**, 1503–1509.

7 *Mesostructure and dynamics in liquids and solutions: University of Bristol, UK, 18-20th September 2013*, Royal Society of Chemistry, Cambridge, 2013, p. 650.

8 M. Požar, A. Kerasidou, B. Lovrinčević, L. Zoranić, M. Mijaković, T. Primorac, F. Sokolić, V. Teboul and A. Perera, *The Journal of Chemical Physics*, 2016, **145**, 144502.

9 D. Corradini, Z. Su, H. E. Stanley and P. Gallo, *The Journal of Chemical Physics*, 2012, **137**, 184503.

10 C. Corsaro, E. Fazio and D. Mallamace, *The Journal of Chemical Physics*, 2019, **150**, 234506.

11 D. Subramanian, C. T. Boughter, J. B. Klauda, B. Hammouda and M. A. Anisimov, *Faraday Discussions*, 2013, **167**, 217–238.

12 A. Perera and B. Kežić, *Faraday Discussions*, 2013, **167**, 145–158.

13 J.-H. Guo, Y. Luo, A. Augustsson, S. Kashtanov, J.-E. Rubensson, D. K. Shuh, H. Ågren and J. Nordgren, *Physical Review Letters*, 2003, **91**, 157401.

14 A. Triolo, O. Russina, H. J. Bleif and E. Di Cola, *Journal of Physical Chemistry B*, 2007, **111**, 4641–4644.

15 F. Ferdeghini, Q. Berrod, J. M. Zanotti, P. Judeinstein, V. G. Sakai, O. Czakkel, P. Fouquet and D. Constantin, *Nanoscale*, 2017, **9**, 1901–1908.

16 A. P. Abbott, G. Capper, D. L. Davies, R. K. Rasheed and V. Tambyrajah, *Chemical Communications*, 2003, 70–71.

17 A. Faraone, D. V. Wagel, G. A. Baker, E. C. Novak, M. Ohl, D. Reuter, P. Lunkenheimer, A. Loidl and E. Mamontov, *Journal of Physical Chemistry B*, 2018, **122**, 1261–1267.

18 O. Borodin, L. M. Suo, M. Gobet, X. M. Ren, F. Wang, A. Faraone, J. Peng, M. Olguin, M. Schroeder, M. S. Ding, E. Gobrogge, A. V. Cresce, S. Munoz, J. A. Dura, S. Greenbaum, C. S. Wang and K. Xu, *Acs Nano*, 2017, **11**, 10462–10471.

19 G. Horwitz, E. Härk, P. Y. Steinberg, L. P. Cavalcanti, S. Risse and H. R. Corti, *ACS Nano*, 2021.

20 L. Dougan, R. Hargreaves, S. P. Bates, J. L. Finney, V. Reat, A. K. Soper and J. Crain, *The Journal of Chemical Physics*, 2005, **122**, 174514.

21 A. K. Soper and J. L. Finney, *Physical Review Letters*, 1993, **71**, 4346.

22 W. S. Price, H. Ide and Y. Arata, *The Journal of Physical Chemistry A*, 2003, **107**, 4784–4789.

23 F. Mallamace, C. Corsaro, D. Mallamace, C. Vasi, S. Vasi and H. E. Stanley, *The Journal of Chemical Physics*, 2016, **144**, 064506.

24 C. Corsaro, J. Spooren, C. Branca, N. Leone, M. Broccio, C. Kim, S. H. Chen, H. E. Stanley and F. Mallamace, *Journal of Physical Chemistry B*, 2008, **112**, 10449–10454.

25 J. S. Gardner, G. Ehlers, A. Faraone and V. G. Sakai, *Nature Reviews Physics*, 2020, 1–14.

26 C. E. Bertrand, W.-S. Chiang, M. Tyagi and S.-H. Chen, *The Journal of Chemical Physics*, 2013, **139**, 014505.

27 A. Faraone, K. Hong, L. R. Kneller, M. Ohl and J. R. D. Copley, *The Journal of Chemical Physics*, 2012, **136**, 104502.

28 C. E. Bertrand, J. L. Self, J. R. D. Copley and A. Faraone, *The Journal of Chemical Physics*, 2016, **145**, 014502.

29 C. E. Bertrand, J. L. Self, J. R. D. Copley and A. Faraone, *The Journal of Chemical Physics*, 2017, **146**, 194501.

30 A. Faraone, D. V. Wagle, G. A. Baker, E. C. Novak, M. Ohl, D. Reuter, P. Lunkenheimer, A. Loidl and E. Mamontov, *The Journal of Physical Chemistry B*, 2018, **122**, 1261–1267.

31 T. Yamaguchi, A. Faraone and M. Nagao, *The Journal of Physical Chemistry B*, 2019, **123**, 239–246.

32 C. Corsaro, J. Spooren, C. Branca, N. Leone, M. Broccio, C. Kim, S.-H. Chen, H. E. Stanley and F. Mallamace, *The Journal of Physical Chemistry B*, 2008, **112**, 10449–10454.

33 C. J. Glinka, J. G. Barker, B. Hammouda, S. Krueger, J. J. Moyer and W. J. Orts, *Journal of Applied Crystallography*, 1998, **31**, 430–445.

34 J. R. D. Copley and J. C. Cook, *Chemical Physics*, 2003, **292**, 477–485.

35 N. Rosov, S. Rathgeber and M. Monkenbusch, in *Neutron Spin Echo spectroscopy at the NIST Center for Neutron Research*, ed. P. Cebe, B. S. Hsiao and D. J. Lohse, 2000, vol. 739, pp. 103–116.

36 S. R. Kline, *Journal of Applied Crystallography*, 2006, **39**, 895–900.

37 F. Mezei, *Lecture Notes in Physics*, 1980.

38 F. Mezei, C. Pappas and T. Gutberlet, *Neutron spin echo spectroscopy: Basics, trends and applications*, Springer Science & Business Media, 2002, vol. 601.

39 R. T. Azuah, L. R. Kneller, Y. Qiu, P. L. W. Tregenna-Piggott, C. M. Brown, J. R. D. Copley and R. M. Dimeo, *Journal of Research of the National Institute of Standards and Technology*, 2009, **114**, 341.

40 H. J. C. Berendsen, D. van der Spoel and R. van Drunen, *Computer Physics Communications*, 1995, **91**, 43–56.

41 W. L. Jorgensen and J. Tirado-Rives, *Journal of the American Chemical Society*, 1988, **110**, 1657–1666.

42 W. L. Jorgensen, J. Chandrasekhar, J. D. Madura, R. W. Impey and M. L. Klein, *The Journal of Chemical Physics*, 1983, **79**, 926–935.

43 B. Hess, H. Bekker, H. J. C. Berendsen and J. G. E. M. Fraaije, *Journal of Computational Chemistry*, 1997, **18**, 1463–1472.

44 S. Miyamoto and P. A. Kollman, *Journal of Computational Chemistry*, 1992, **13**, 952–962.

45 U. Essmann, L. Perera, M. L. Berkowitz, T. Darden, H. Lee and L. G. Pedersen, *The Journal of Chemical Physics*, 1995, **103**, 8577–8593.

46 S. Nosé, *The Journal of Chemical Physics*, 1984, **81**, 511–519.

47 S. Nosé, *Molecular Physics*, 1984, **52**, 255–268.

48 W. G. Hoover, *Physical Review A*, 1985, **31**, 1695–1697.

49 H. J. C. Berendsen, J. P. M. v. Postma, W. F. van Gunsteren, A. R. H. J. DiNola and J. R. Haak, *The Journal of Chemical Physics*, 1984, **81**, 3684–3690.

50 N. P. Walter, A. Jaiswal, Z. Cai and Y. Zhang, *Computer Physics*

Communications, 2018, **228**, 209–218.

51 M. Bée, *Quasielastic neutron scattering*, CRC Press, 1988.

52 A. M. Gaspar, S. Busch, M.-S. Appavou, W. Haeussler, R. Georgii, Y. Su and W. Doster, *Biochimica et Biophysica Acta (BBA)-Proteins and Proteomics*, 2010, **1804**, 76–82.

53 A. Perera, F. Sokolić, L. Almasy and Y. Koga, *The Journal of Chemical Physics*, 2006, **124**, 124515.

54 T. M. Bender and R. Pecora, *Journal of Physical Chemistry*, 1989, **93**, 2614–2620.

55 N. W. Ashcroft and D. C. Langreth, *Phys. Rev.*, 1967, **156**, 685–692.

56 T. José, L. Alenka and L. Stéphane, *Journal of Physics: Condensed Matter*, 2006, **18**, S2353.

57 T. A. Pascal and W. A. Goddard III, *The Journal of Physical Chemistry B*, 2012, **116**, 13905–13912.

58 A. Perera, F. Sokolić and L. Zoranić, *Physical Review E*, 2007, **75**, 060502.

59 A. B. Bhatia and D. E. Thornton, *Physical Review B-Solid State*, 1970, **2**, 3004–3012.

60 A. B. Bhatia, D. E. Thornton and N. H. March, *Physics and Chemistry of Liquids*, 1974, **4**, 97–111.

61 G. C. Benson and P. J. Darcy, *Journal of Chemical and Engineering Data*, 1982, **27**, 439–442.

62 H. A. Zarei, F. Jalili and S. Assadi, *Journal of Chemical and Engineering Data*, 2007, **52**, 2517–2526.

63 M. J. Assael, E. Charitidou and W. A. Wakeham, *International Journal of Thermophysics*, 1989, **10**, 793–803.

64 H. Kitajima, N. Kagawa, H. Endo, S. Tsuruno and J. W. Magee, *Journal of Chemical and Engineering Data*, 2003, **48**, 1583–1586.

65 T. Kuroki, N. Kagawa, H. Endo, S. Tsuruno and J. W. Magee, *Journal of Chemical and Engineering Data*, 2001, **46**, 1101–1106.

66 W. D. T. Dale, P. A. Flavelle and P. Kruus, *Canadian Journal of Chemistry-Revue Canadienne De Chimie*, 1976, **54**, 355–366.

67 N. Micali, S. Trusso, C. Vasi, D. Blaudez and F. Mallamace, *Physical Review E*, 1996, **54**, 1720–1724.

68 F. Mallamace, C. Branca, C. Corsaro, N. Leone, J. Spooren, H. E. Stanley and S.-H. Chen, *The Journal of Physical Chemistry B*, 2010, **114**, 1870–1878.

69 Z. J. Derlacki, A. J. Easteal, A. V. J. Edge, L. A. Woolf and Z. Roksandic, *The Journal of Physical Chemistry*, 1985, **89**, 5318–5322.

70 Y. H. Zhou and G. H. Miller, *Physical Review E*, 1996, **53**, 1587–1601.

71 E. G. Pérez, D. Gonzalez-Salgado and E. Lomba, *Fluid Phase Equilibria*, 2021, **528**, 112840.

72 X. Tian, Z. Yang, B. Zhou, P. Xiu and Y. Tu, *The Journal of Chemical Physics*, 2013, **138**, 204711.

73 M. Matsugami, R. Yamamoto, T. Kumai, M. Tanaka, T. Umecky and T. Takamuku, *Journal of Molecular Liquids*, 2016, **217**, 3–11.

74 S. Z. Mikhail and W. R. Kimel, *Journal of Chemical & Engineering Data*, 1961, **6**, 533–537.

75 S. Song and C. Peng, *Journal of Dispersion Science and Technology*, 2008, **29**, 1367–1372.

76 Y. Zhai, P. Luo, M. Nagao, K. Nakajima, T. Kikuchi, Y. Kawakita, P. A. Kienzle, Y. Z and A. Faraone, *Physical Chemistry Chemical Physics*, 2021, **23**, 7220–7232.

77 A. Arbe, G. J. Nilsen, J. R. Stewart, F. Alvarez, V. G. Sakai and J. Colmenero, *Physical Review Research*, 2020, **2**, 022015.

78 P. Luo, Y. Zhai, E. Senses, E. Mamontov, G. Xu, Y. Z and A. Faraone, *The Journal of Physical Chemistry Letters*, 2020, **11**, 8970–8975.

79 T. Yamaguchi and A. Faraone, *The Journal of Chemical Physics*, 2017, **146**, 244506.

80 T. José, L. Alenka and L. Stéphane, *Journal of Physics: Condensed Matter*, 2006, **18**, S2353.

81 H. E. Stanley and J. Teixeira, *The Journal of Chemical Physics*, 1980, **73**, 3404–3422.

82 T. Yamaguchi, *The Journal of Chemical Physics*, 2017, **146**, 094511.